Oscillation-induced sand ripples in a circular geometry

Germain Rousseaux*
Laboratoire J.-A. Dieudonné, Université de Nice–Sophia Antipolis, UMR 6621 CNRS-UNSA, Parc Valrose, 06108 Nice Cedex 02, France

Joachim Kruithof,† Patrice Jenffer,‡ and José Eduardo Wesfreid§
Physique et Mécanique des Milieux Hétérogènes, UMR 7636, CNRS-ESPCI, 10, Rue Vauquelin, 75231 Paris Cedex 05, France
(Received 18 November 2007; published 7 July 2008)

This study deals with the observation of sand ripples in a circular geometry under oscillatory flow. We characterize the observed patterns as a function of the excitation parameters. We report the time evolution of the corrugated front invading the flat bed. These experiments reveal unambiguously, because of the gradient of shear stress, the existence of two separated thresholds: one for grain motion and the other for the appearance of ripples. In addition, we display the phase diagram of this instability as a function of the Froude number and a Reynolds number.

DOI: 10.1103/PhysRevE.78.016302 PACS number(s): 47.57.Gc, 47.20.Ma, 47.54.De

Ripples are sand patterns which are built by the to and fro motion induced by surface water waves at the fluid-granular interface on the beach. Historically, the first laboratory experiments on underwater sand ripples were performed by De Candolle in 1882 and Darwin in 1883 using oscillating circular tanks filled with water, at the bottom of which they put a layer of sand [1,2]. More recently, Fermigier and Jenffer used the same circular geometry [3]. Bagnold [4], who designed a setup with an oscillating plate covered by a layer of sand in static water, observed two types of pattern: rolling-grain ripples (small patterns with grains moving back and forth at the interface between sand and water) and vortex ripples (larger patterns with a vortex detaching from the crest taking out grains from the neighboring sand structures). Underwater rolling-grain ripples always evolve toward vortex ripples, and both feature a transient vortex [5–9]. It seems that De Candolle and Darwin observed only vortex ripples whereas Fermigier and Jenffer saw both rolling-grain and vortex ripples [3]. In the context of a more general experimental study on underwater ripples in our laboratory, we reproduce these experiments in a very controlled manner in order to obtain quantitative results especially about the onset of the instability.

The principle of the setup is similar to the one used in [3]. A bottom plate with a circular tank of radius R fixed over it is driven by a centered axis which oscillates azimuthally at a fixed displacement amplitude A and frequency f. We put in a layer of height h of monodisperse spherical glass beads of diameter d (relative density with respect to water $\rho_s/\rho_f = 2.49$). Then we fill the tank with water (kinematic viscosity $\nu = 10^{-6}$ m^2 s^{-1}) of height H. This closed receptacle preserves mass conservation and the circular geometry gives spatially periodic boundary conditions. Our setup is made of a cylinder in Altuglass of radius $R_{\mathrm{ext}} = 11$ cm and of height $h_c = 19.5$ cm. The circular bottom plate is made of polyvinyl chloride. The circular neon lamp used for lighting is movable in height and avoids optical inhomogeneities along the perimeter. Pictures are taken with a charge-coupled device camera which is mounted on the top of the oscillating setup. Due to the oscillatory motion of the tank and for both the plane and cylindrical geometry, a Stokes boundary layer of thickness $\delta = \sqrt{\nu/\pi f}$ is present at the interface between the water and the bed of glass beads and is at the origin of ripple formation [5,6]. In addition, a similar boundary layer exists on the inner vertical face of the circular tank but does not contribute to the observed radial patterns. This kind of geometry was studied recently because of the occurrence of other granular instabilities and secondary flows [10,11]. We will not perform a detailed calculation of the secondary flow created by the granular bed oscillation and spin-up effects, but it is easy to predict the existence of a toroidal pulsed structure, as was studied in continuous rotation in [12]. The trajectories of particles show that the radial component of the flow structure is very weak. This circular flow induced by the walls puts the grains in movement and the azimuthal velocity varies linearly with the radius. Hence, we have a system where one can observe the influence of a radial gradient of shear amplitude.

The visualizations of the sand-water interface with the camera on top are shown in Fig. 1. In Fig. 1(a) we distinguish the flat initial state. After starting the oscillations, we can observe at the outer region of the disk ($r = R_{\mathrm{ext}}$) a first type of structure that we identify as rolling-grain ripples in Fig. 1(b). In Fig. 1(c), after a while, we notice the transition from rolling-grain ripples to deeper structures growing inward, which are vortex ripples. Then, in Fig. 1(d), the final state is characterized by the presence of an inner circle without structures, and radial ripples.

At a distance r from the tank center, the mean wavelength of the radial vortex ripples is obtained as the ratio between the perimeter $P = 2\pi r$ and the number of ripples N. The existence of a final radial state implies that the number of vortex ripples is constant whatever is the radius r [dislocations which are features of transitory regimes or of three-dimensional (3D) effects are absent here], $\langle \lambda_f(r) \rangle = \frac{P}{N} = \frac{2\pi r}{N}$

*Germain.Rousseaux@unice.fr
†kruithof@pmmh.espci.fr
‡patrice@pmmh.espci.fr
§wesfreid@pmmh.espci.fr

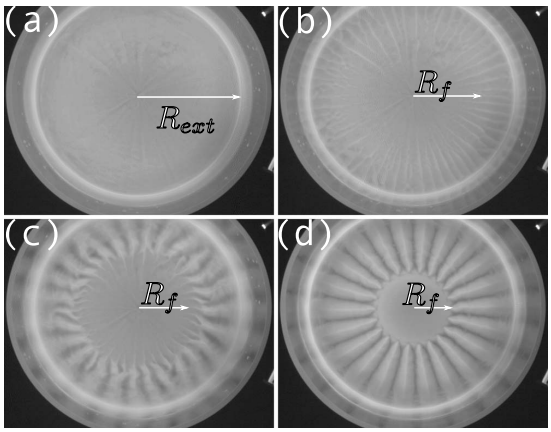

FIG. 1. Primary patterns seen from above with an attached camera in the setup: (a) initial state, (b) rolling-grain ripples (after 50 s), (c) transition (after 100 s), and (d) saturated vortex ripples (after 10^3 s). Parameters are $f=1$ Hz, $A=3$ cm, $d\simeq 110$ μm. R_f is the radius of the ripple front. R_{ext} is the radius of the cylindrical tank.

$=\text{const}\times r$. Moreover, the amplitude of motion is proportional to the radius. One concludes that the final wavelength of the vortex ripples is proportional to the oscillations' amplitude $\lambda_f(r)\simeq A$, as predicted by Longuet-Higgins [13] and observed in many experiments, especially in [5] where $\lambda_f=4/3A$. This result, inherent to the circular geometry, was observed as early as 1882 by De Candolle [1]. Hence, the wavelength increases linearly from the instability threshold to the external radius R_{ext} [Fig. 1(d)]. These observations strengthen the argument about the vortex ripple wavelength selection, where $\lambda\sim A$, and clarify the debate about the final wavelength of vortex ripples, as several correlations have been proposed for the final wavelength of vortex ripples (some with a proportionality law) [14].

Figure 2 shows several views of the final vortex ripple state. As noticed before, an internal circular zone without structure is present [Fig. 2(a)]. However, small deformations (which we call streaks in the following) induced during the flattening procedure are present but they do not evolve with time. Hence, we are sure that no transport is present below

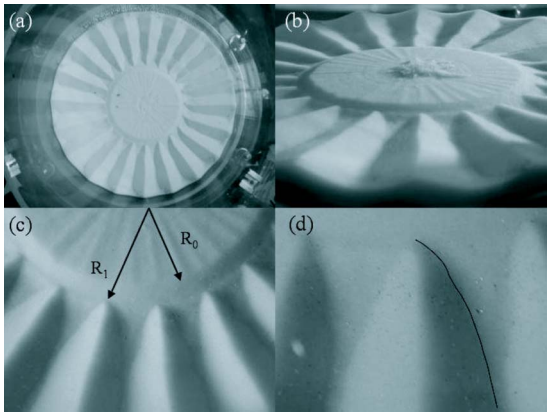

FIG. 2. (Color online) Description of the final state after 18 h: (a) threshold for movement, (b) dust in the center of the tank, (c) zoom on both internal radii, and (d) zoom on the internal part of a ripple.

the inner radius. In addition, one can see an accumulation of dust in the very center of the latter zone. A rotating fluid in a circular tank features a secondary pulsed flow directed from the center toward the walls inside the boundary layer, which deposits particles in the center. If we focus on the edge of the nonstructured region [Figs. 2(b) and 2(c)], we can see two characteristic radii: the first one R_0 corresponds to the absence of grain motion for $r\ll R_0$; the second one R_1 is situated at the end of a descending slope which starts on a kind of promontory delimited by the first radius R_0. Between R_0 and R_1, the absence of the initial streaks shows the existence of grain motion but without ripple formation: the streaks disappear throughout the ripple formation process by both the grain motion and the inner invasion of the patterns. This demonstrates the existence of two distinct thresholds for oscillating flow over a sand bed, which we confirmed by image subtraction between successive pair of pictures taken with the camera (not reported here). R_0 corresponds to the threshold for grain motion whereas R_1 corresponds to the stability threshold for the periodic patterns of ripples. Hence, theories of ripple formation should distinguish between the two. Very little experimental evidence of this gap between thresholds has been published so far [15–17]. Moreover, the observation of the region close to R_1 reveals a "shark tooth" form of the ripples [Fig. 2(d)]. From these observations we can estimate the critical Shields number to put grains in motion. Indeed, the Shields number, which is the ratio between the shear force on the grains and their apparent weight, is defined by $\text{Sh}(r)\simeq\frac{\tau(r)d^2}{\Delta\rho g d^3}\simeq\frac{\mu A(r)f}{\Delta\rho g d\delta}\simeq\frac{\rho_f}{\Delta\rho g d}\nu^{1/2}f^{3/2}\frac{A_{\text{ext}}}{R_{\text{ext}}}r$. $A(r)=(rA_{\text{ext}})/R_{\text{ext}}$ is the local amplitude of oscillation expressed as a function of the external radius R_{ext} and amplitude A_{ext}. The velocity gradient in the shear stress $\tau(r)$ is estimated from the ratio of the velocity $U\simeq 2\pi Af$ and the Stokes boundary layer thickness $\delta=\sqrt{\nu/(\pi f)}$. It is legitimate to ask if the grain transport in the descending region could not be due to a secondary flow, with the grains transported radially beyond R_1. However, if the equivalent radial Shields number (secondary flow plus centrifugal force) were bigger than the azimuthal one, one would observe an inclined surface with an increased level toward the outer radius. We observe the contrary. Moreover, one may wonder if the radius R_1 really corresponds to the stability threshold as one would measure it in a plane geometry. As a matter of fact, it is possible that the threshold can be modified by the fact that the vortex associated with the vortex ripples could diffuse toward the center of the tank by viscosity. If this were the case, the size of the diffused layer would scale with the Stokes layer, which is negligible compared to the radius R_1, which is 100 times larger. Moreover, vortex ripples correspond to finite-amplitude perturbations of the sand bed related to the inertial separation of the flow, and it is possible that the stability threshold could be different than in the case of small rolling-grain ripples. In any case, the circular geometry is a good candidate in order to study with more detail the threshold for both grain motion and pattern formation and work is in progress in order to compare with the plane geometry [17]. We would like to underline that previous authors have reported the existence of two thresholds in plane geometry [15,16]. However, the time of observation is not given in their experiments. Indeed, the

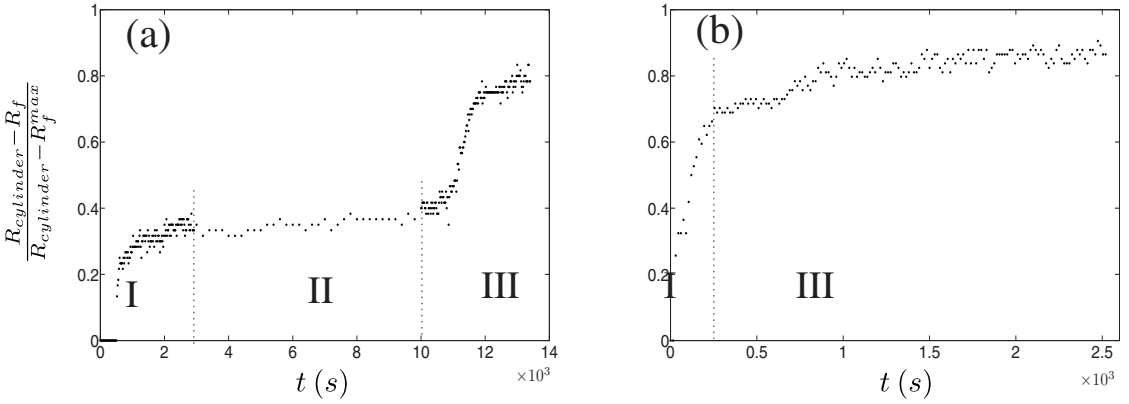

FIG. 3. Temporal evolution of $(R_{ext}-R_f)/(R_{ext}-R_f^{max})$. The parameters are $d=200\pm 50$ μm, (a) $A=2$ cm, $f=1$ Hz (Fr=2.2, $\mathrm{Re}_\delta=71$), and (b) $A=1.5$ cm, $f=1.5$ Hz (Fr=2.5, $\mathrm{Re}_\delta=65$). The typical time for vortex ripple formation is 1000 s for (a) and 300 s for (b).

rolling-grain ripples can appear on very long time scales, hours or even days. The major advantage of the circular geometry is to impose a gradient of excitation which allows us to determine both thresholds accurately.

We follow the time evolution of the position of *the instability front* R_f associated with one ripple (Fig. 1), which grows inward with time until it reaches the critical radius $(R_f=R_1)$. A camera placed above the cylindrical container takes a picture every 15 s and we measure the front position R_f of one ripple on each picture. R_f^{max} is defined as R_f after $t_{max}=2\times 10^5$ s (=2.3 days) of evolution. It is measured at the end of each experimental run but we present only measurements in the initial stage of growth $(t\ll t_{max})$. We consider that, from the experimental point of view, $R_f^{max}\simeq R_1$. Figures 3 and 4 show three different time evolutions of $(R_{ext}-R_f)/(R_{ext}-R_f^{max})$. This parameter is proportional to the radial length of the ripples and is relevant since the ripples grow toward the center of the tank.

The parameter set in Fig. 3(a) is close to the threshold of the instability (see below). From the beginning of the experiment Fig. 3(a) to $t\simeq 2.5\times 10^3$ s we observe the initial growth of the rolling-grain ripples (phase I). Then, we observe quasistability of the rolling-grain ripples for 7×10^3 s (phase II). During that time, the wavelength is constant as is R_f. At $t\simeq 10^4$ s, the transition from rolling-grain ripples to vortex ripples begins (phase III). We recall here that the initial flat bed is prepared with a flattening procedure [6]. This flattening procedure must leave no defects (bump or hole) in the sand, since any defect with a sufficient height [4,18] initiates a transition from rolling-grain ripples to vortex ripples with propagating fronts. Furthermore, a defectless sand surface is a necessary condition to observe the plateau (phase II) for a long time. Any defect, even if not big enough to trigger the transition to vortex ripples, can modify the ripple dynamics and hide the plateau. As the initial size of the rolling-grain ripples is tiny, to obtain precise experimental results we zoom in on the active zone of the initial stages of growth. The second part of the dynamics is described using another experiment with the same parameters $(\mathrm{Fr},\mathrm{Re}_\delta)$, where we film the whole apparatus. In other experiments farther from the threshold, the plateau with $R_f=$const (phase II) is absent since the transition from rolling-grain to vortex ripples is faster. With the parameter set of Fig. 3(b), the rolling-grain ripple state lasts approximately 200 s and vortex ripples grow almost immediately. Like some other parameters, such as height and wavelength [5,6,8,9], R_f rises abruptly when the front of the vortex ripple instability reaches the spot of study. In Fig. 4 we present a more detailed study even nearer the onset of the instability. With these parameters, the system exhibits a very slow dynamics.

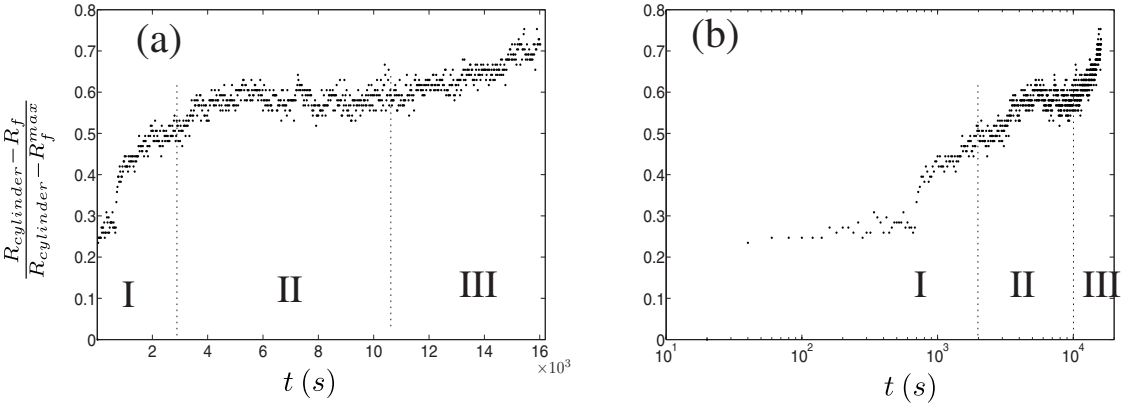

FIG. 4. Evolution of (a) $(R_{ext}-R_f)/(R_{ext}-R_f^{max})$ vs time; (b) R_f/R_f^{max} vs $\log_{10}(t)$. The parameters are $d=200\pm 50$ μm, $A=1.9$ cm, $f=1$ Hz, Fr=2.1, and $\mathrm{Re}_\delta=67$.

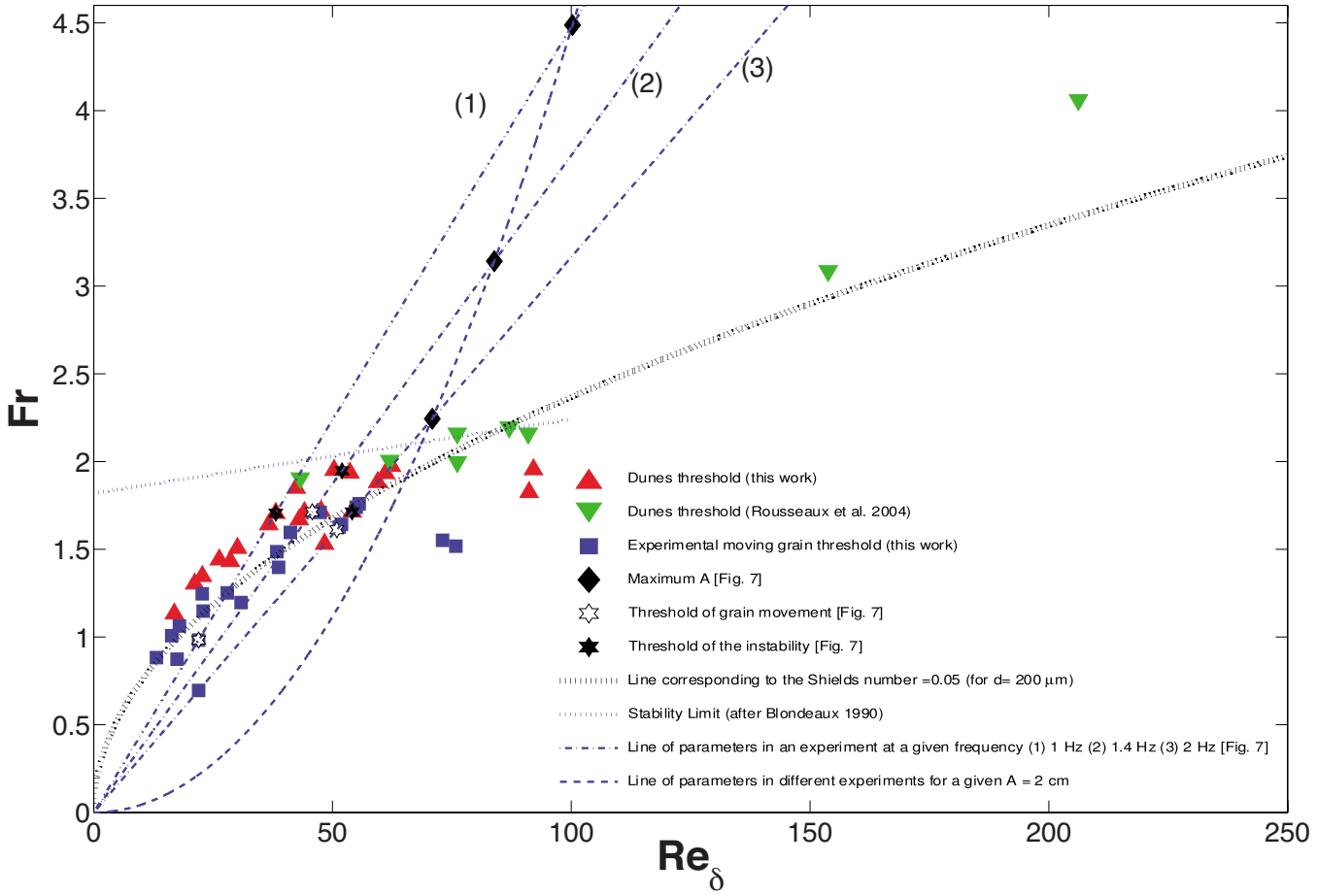

FIG. 5. (Color online) Final critical radius and moving grains threshold compared with Shields threshold in Re$_\delta$-Fr diagram. Experiments made at a given frequency have outer and critical Re$_\delta$-Fr on the same line. This is not the case for experiments at constant amplitude and varying frequency. The data of Rousseaux *et al.* and Blondeaux are extracted from [6] and [19], respectively.

If we plot $R_f/R_f^{\max}$ versus $\log_{10}(t)$ we can find a logarithmic evolution of R_f for a part of the data set (phase I in Fig. 3). A power-law fit gives good agreement with this data either (Fig. 4). An attempt to fit the growth in parameters from Figs. 3 and 4 with an exponential saturation $[1-\exp(t/\tau)]$ failed. The evolution of this 3D parameter (R_f) depending on the distance to threshold is comparable with that of other 2D parameters like the wavelength or the height; see Fig. 2(a) in [6]. We show only the initial part of Figs. 3 and 4 but at the end of the experiment we reach $R_f^{\max}$.

On a very long time scale ($\sim 10^5$ s) we measure two critical radii (Fig. 2) defining two thresholds. (1) The threshold of the region with grains at rest defines the critical Shields number to put these grains in motion (R_0 in Fig. 2); (2) at a larger radius, in the region with grains in motion, appears the onset of sand ripples (R_1 in Fig. 2). Let us recall that, in our experiments, the cylindrical geometry imposes the requirement that the amplitude grows linearly with the radius ($A=\theta r$). We choose as control parameters of this instability the Froude number Fr and the Reynolds number defined with the boundary layer thickness Re$_\delta$ as in previous theoretical works [19] and experiments [6]. These dimensionless numbers are defined according to $\mathrm{Fr}=\frac{\sqrt{\rho_f}A\omega}{\sqrt{(\rho_s-\rho_f)gd}}$ and $\mathrm{Re}_\delta=\frac{U\delta}{\nu}=\frac{2A}{\delta}$.

As the Froude number $\mathrm{Fr}=\sqrt{\frac{\pi\nu}{(s-1)gd}}\mathrm{Re}_\delta\sqrt{f}$ with $s=\rho_s/\rho_f$ is linearly dependent on Re$_\delta$, we scan the phase space (Fig. 5) of the instability by choosing f=const. This implies an exploration of the phase space on straight lines with different slopes. In that case, both thresholds are located on the same line (f constant with linearly varying A). We choose to use high frequencies (f=4.5 Hz) to stay in the low-Re$_\delta$ region. We obtain tiny vortex ripples (Fig. 6). The lower f, the lower the slope. This enables us to obtain higher values of Re$_\delta$. In the high-Re$_\delta$ region, to reach the threshold of the instability implies the use of a big amplitude with decreasing frequency. In Fig. 5, we display results both from published experiments

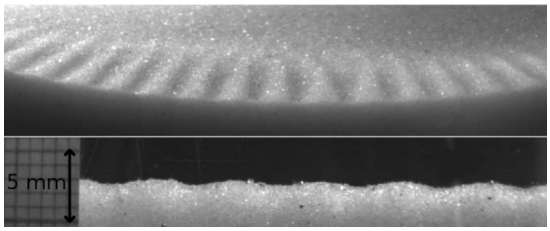

FIG. 6. Side view and front view of vortex ripples using low-amplitude high-frequency parameters: $d=200\pm50$ μm, $A=0.3$ cm, $f=4.5$ Hz, Re$_\delta$=22, and Fr=1.5.

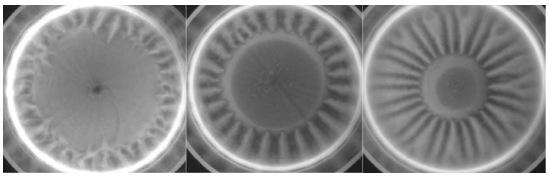

FIG. 7. Experiments at constant amplitude $A=2$ cm, $d=200\pm50$ μm, after 6×10^3 s. From left to right, outer values are $f=1$ Hz (Fr=2.2, $\mathrm{Re}_\delta=71$), $f=1.4$ Hz (Fr=3.1, $\mathrm{Re}_\delta=84$), and $f=2$ Hz (Fr=4.5, $\mathrm{Re}_\delta=100$). The number of vortex ripples is constant as raising the frequency sets the parameters farther from the threshold of the instability (see Fig. 5). The experimental critical Shields number for grain motion is (from left to right) 0.08, 0.08, and 0.07.

in an annular geometry [6], and from current experiments in a circular geometry, which show that thresholds for the instability are similar. In addition, we show a line of constant Shields number. We choose Sh=0.05 as a typical value recognized in the literature for the onset of grain motion [14]. To assess the effect of frequency, we made experiments at a constant outer amplitude. In that case (A=const), the Froude number can be written as a quadratic function of Re_δ: $\mathrm{Fr}=\frac{\nu}{2\sqrt{(s-1)gd}}\frac{1}{A}\mathrm{Re}_\delta^2$. For A=const, we remarked visually that the more the frequency increases the more the thresholds (grain movement and instability onsets) are separated, as displayed in Fig. 7, where a constant amplitude is used; we deduced the critical Shields number experimentally, which is around 0.08. However, as we reach amplitudes such that $A\sim R_{\mathrm{ext}}$, there is a competition between two length scales. In that case, the results show that the ripples reach a critical radius lower than expected, which is also the case for moving grains (Fig. 5).

As a conclusion, we looked for the evolution of a granular bed submitted to an oscillating flow. We demonstrated that the wavelength is proportional to the amplitude of oscillation in the final state of the vortex ripples regime using a circular geometry. This scaling was reported by De Candolle as early as 1882 with a similar setup. In our study we looked for the stabilization of the inner radius with time and, in consequence, we can really separate two different thresholds (one for grain movement and the other for ripple stability) in the same experiment. Hence, we report experiments where one is sure to have reached the final state. Indeed, among the large numbers of correlations which have been proposed in the literature so far, the measurements do not prove that one has really reached a final state because of the side visualizations with planar geometry in wave tanks. The influence of centrifugal forces and curvature seems to invalidate the use of circular geometry to study the initial streak formation, individual grain motion, and secondary sand instabilities. However, we think that these effects do not invalidate the generality of our results, since they compare well with previous findings in planar geometries.

The authors are grateful to Denis Vallet, Olivier Brouard, and Christian Baradel for technical help. This work was supported by the A.C.I. "Jeunes chercheurs" Grant No. 2314.

[1] C. De Candolle, Arch. Sci. Phys. Nat. **3**, 253 (1882).
[2] G. H. Darwin, Proc. R. Soc. Edinburgh **36**, 18 (1883).
[3] M. Fermigier and P. Jenffer, Phys. Fluids **14**, S9 (2002).
[4] R. A. Bagnold, Proc. R. Soc. London, Ser. A **187**, 1 (1946).
[5] A. Stegner and J. E. Wesfreid, Phys. Rev. E **60**, R3487 (1999).
[6] G. Rousseaux, A. Stegner, and J. E. Wesfreid, Phys. Rev. E **69**, 031307 (2004).
[7] G. Rousseaux, H. Yoshikawa, A. Stegner, and J. E. Wesfreid, Phys. Fluids **16**, 1049 (2004).
[8] G. Rousseaux, H. Caps, and J. E. Wesfreid, Eur. Phys. J. E **13**, 213 (2004).
[9] G. Rousseaux, Phys. Rev. E **74**, 066305 (2006).
[10] F. Zoueshtiagh and P. J. Thomas, Phys. Rev. E **61**, 5588 (2000).
[11] H. Caps and N. Vandewalle, Phys. Rev. E **68**, 031303 (2003).
[12] C. Nore, L. S. Tuckerman, O. Daube, and S. Xin, J. Fluid Mech. **477**, 51 (2003).
[13] M. S. Longuet-Higgins, J. Fluid Mech. **107**, 1 (1981).
[14] P. Nielsen, *Coastal Bottom Boundary Layers and Sediment Transport* (World Scientific, Singapore, 1992).
[15] R. Carstens, F. M. Neilson, and H. D. Altinbilek, U.S. Army Corps of Engineers Coastal Engineering Research Center, Technical Memorandum No. 28, 1969 (unpublished).
[16] K. W. Chan, M. H. I. Baird, and G. F. Round, Proc. R. Soc. London, Ser. A **330**, 537 (1972).
[17] P. Stevenson and R. B. Thorpe, Chem. Eng. Sci. **59**, 1295 (2004).
[18] T. Sekiguchi and T. Sunamura, Coastal Eng. **50**, 231 (2004).
[19] P. Blondeaux, J. Fluid Mech. **218**, 1 (1990).